nature biomedical engineering

ARTICLES

https://doi.org/10.1038/s41551-020-0590-1

Check for updates

Tracking the expression of therapeutic protein targets in rare cells by antibody-mediated nanoparticle labelling and magnetic sorting

Mahmoud Labib[1], Zongjie Wang[2], Sharif U. Ahmed[1], Reza M. Mohamadi[1], Bill Duong[1], Brenda Green[1], Edward H. Sargent[3] and Shana O. Kelley[1,2,4]✉

Molecular-level features of tumours can be tracked using single-cell analyses of circulating tumour cells (CTCs). However, single-cell measurements of protein expression for rare CTCs are hampered by the presence of a large number of non-target cells. Here, we show that antibody-mediated labelling of intracellular proteins in the nucleus, mitochondria and cytoplasm of human cells with magnetic nanoparticles enables analysis of target proteins at the single-cell level by sorting the cells according to their nanoparticle content in a microfluidic device with cell-capture zones sandwiched between arrays of magnets. We used the magnetic labelling and cell-sorting approach to track the expression of therapeutic protein targets in CTCs isolated from blood samples of mice with orthotopic prostate xenografts and from patients with metastatic castration-resistant prostate cancer. We also show that mutated proteins that are drug targets or markers of therapeutic response can be directly identified in CTCs, analysed at the single-cell level and used to predict how mice with drug-susceptible and drug-resistant pancreatic tumour xenografts respond to therapy.

The liquid biopsy, whereby tumour-derived material is collected from the blood, is an emerging replacement for invasive tissue biopsies with great promise for the noninvasive management of cancer. Circulating tumour cells (CTCs) are important targets for liquid biopsy, as they enable the biology and heterogeneity of a tumour to be interrogated[1]. CTCs are rare cells that are shed from primary and metastatic tumour sites into the circulation and are often present at levels as low as one cell per millilitre of blood. Substantial effort has focused on the isolation and counting of CTCs on the basis of their distinctive characteristics, such as surface protein expression[2–5], size[6–8], dielectric properties[9] and invasiveness[10,11]. However, to make liquid-biopsy-based measurements focused on CTCs clinically actionable, it is imperative to move beyond enumeration of these cells and towards the collection of information that informs patient treatment.

Evaluating expression levels and altered proteoforms for proteins that are targets of cancer therapeutics within CTCs would offer an important new capability for liquid-biopsy testing. A key advantage of this type of noninvasive testing is that it can be applied in situations where tissue biopsy is not applicable (for example, metastatic tumours). Measuring the expression of altered proteoforms in CTCs is a challenging goal, however, given the heterogeneity and rarity of these cells in blood samples. Ensemble measurements of intracellular proteins have been performed using conventional methods such as flow cytometry, immunoblotting and immunohistochemistry[12]. CTCs have been isolated by fluorescence-activated cell sorting (FACS) and analysed for their protein content with multiparameter imaging cytometry[13], and microwestern blot arrays can be used for multiplexed protein analysis[14], but neither approach has been used to evaluate the molecular-level properties of tumours in relation to therapeutic response. Immunohistochemical assays are used in the clinic but are limited to a small number of proteins, owing to the spectral imaging limitations imposed by conventional filter sets. In addition, the low abundance of many intracellular proteins makes their detection using this approach problematic[15].

The majority of protein assays that have been applied to single cells are single-analyte immunoassays; however, newer formats have improved multiplexing using fluorescent proteins[16], DNA-barcoded antibodies and barcode sequencing[17–20], and metal-isotope-labelled antibodies for mass-cytometry applications[21]. In addition, single-molecule enzyme-linked immunosorbent assays (SiMOA)[22] and plasmonic enzyme-linked immunosorbent assay[23] have enabled the analysis of proteins with remarkable sensitivities. However, these methods are primarily limited to the analysis of free[18–20,23] and cell-surface proteins[17], and require on-chip cell lysis[24] or complex sequencing-based analysis[17]. Recently, imaging mass cytometry has shown a great potential for multiplexed analysis of proteins in liquid biopsies from metastatic prostate cancer patients[25]. Microfluidic western blotting has enabled highly specific single-cell analysis of proteins from low starting cell numbers, particularly when integrated with FACS[26], and was recently used to assay small numbers of patient-derived CTCs[27]. However, this type of approach requires a complex workflow and separate capture-and analysis technologies that may cause phenotypic drift.

We recently developed a magnetic ranking cytometry approach to analyse the expression of cell-surface proteins in rare bloodborne CTCs[28]. However, the method is not capable of analysing intracellular proteins due to the low magnetic susceptibility of cells achieved after targeting the intracellular proteins with antibodies labelled with magnetic nanoparticles (MNPs). Here we have developed magnetic cell-labelling reagents that can target intracellular proteins and

[1]Department of Pharmaceutical Sciences, University of Toronto, Toronto, Ontario, Canada. [2]Institute for Biomaterials and Biomedical Engineering, University of Toronto, Toronto, Ontario, Canada. [3]Department of Electrical and Computer Engineering, University of Toronto, Toronto, Ontario, Canada. [4]Department of Biochemistry, University of Toronto, Toronto, Ontario, Canada. ✉e-mail: shana.kelley@utoronto.ca

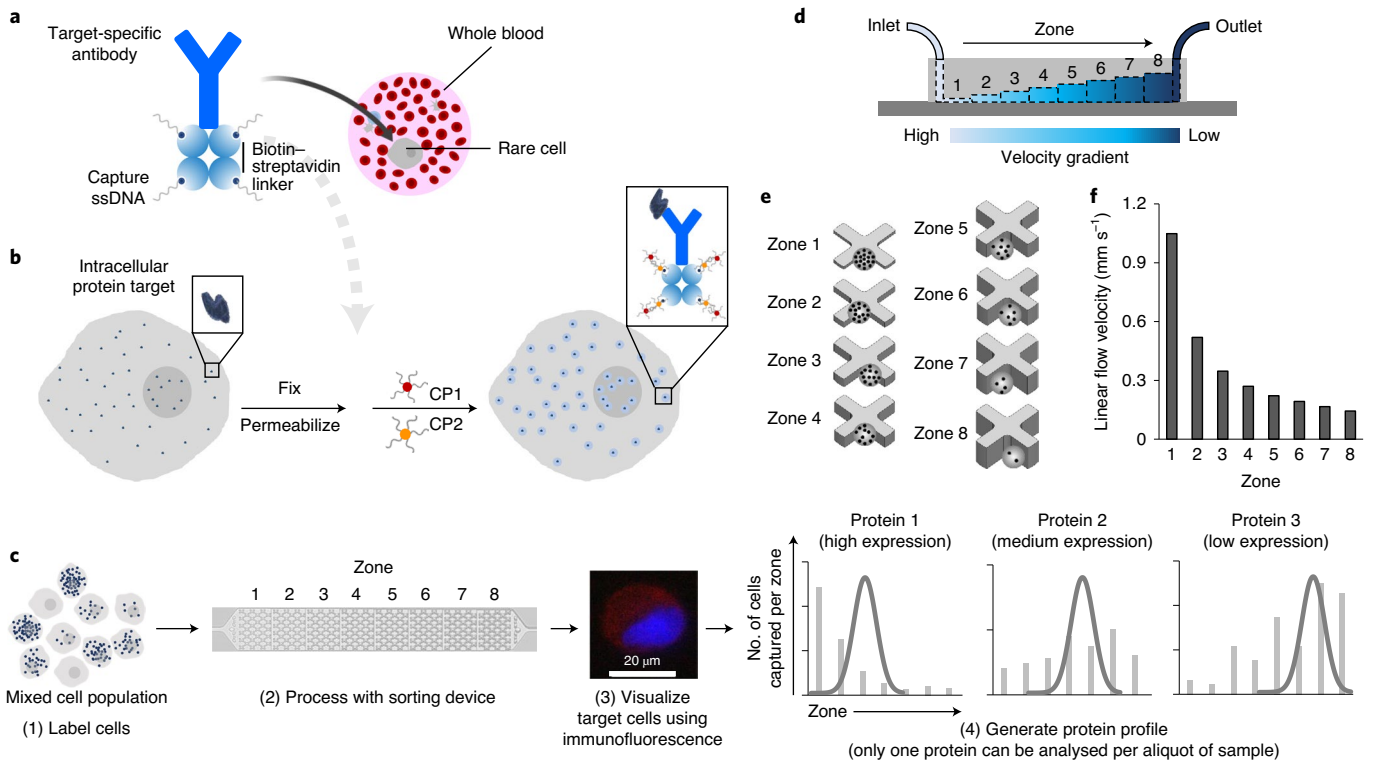

Fig. 1 | The single-cell intracellular protein analysis approach. a, An antibody specific for the target intracellular protein is labelled with streptavidin then modified with biotin-labelled ssDNAs using a biotin–streptavidin linker. **b**, The cells expressing the target intracellular protein are fixed and permeabilized. The cells are incubated with a protein-specific antibody modified with ssDNAs. The ssDNAs are then hybridized with two capture probes (CP1 and CP2), which are composed of complementary DNA sequences modified at one end with MNPs. Aggregates of MNPs are thus formed and trapped within the cells that express the intracellular protein. **c**, The cells are sorted using a microfluidic device, immunostained and counted to generate a profile characteristic for the target protein. Only one protein can be analysed per aliquot of sample. **d**, The microfluidic device features eight sequential zones with increasing heights to facilitate capturing cells with different magnetic content. **e**, Each zone features X-shaped microstructures to create regions of low flow velocity, facilitating cell capture. **f**, The sequential zones feature different average linear velocities of 1×, 0.52×, 0.35×, 0.27×, 0.22×, 0.19×, 0.17× and 0.14× from zone 1 to 8, respectively, at a flow rate of 2 ml h^{-1}.

facilitate magnetic ranking of rare cells according to the expression levels of intracellular proteins. This approach allows the measurement of protein levels within the CTCs of cancer patients, which are important indicators of metastatic potential, and enables a single-cell-level detection of protein markers that are important therapeutic targets.

Results

Our magnetic cell-labelling approach exploits nanoparticle-mediated profiling of cancer cells at the single-cell level according to the expression level of a specific intracellular protein. An antibody specific to an intracellular protein target is chemically modified with streptavidin and then labelled with DNA strands via biotin–streptavidin coupling (Fig. 1a). The cells expressing the intracellular protein are fixed and permeabilized to facilitate the internalization of the labelled antibody. After incubation of the cells with the antibody, each DNA strand is hybridized with a pair of complementary DNA probes appended to iron oxide MNPs, which triggers the formation of large aggregates of MNPs (Fig. 1b). Due to their large size, the aggregates become trapped inside the cells and consequently enhance their magnetic susceptibility, thus providing a generic and highly efficient way to translate the presence of an intracellular protein to a magnetic content. We recently developed a similar strategy for the analysis of intracellular messenger RNAs in rare cells, in which the messenger RNAs were directly targeted with a pair of MNP-labelled complementary DNA probes to create larger clusters of MNPs[29]. Here we designed a family of magnetic cell-labelling reagents to analyse intracellular proteins. Dynamic light scattering measurements demonstrated that combining an antibody labelled with a DNA strand and a pair of MNP-labelled complementary DNA probes produced larger aggregates of MNPs (Supplementary Fig. 1), a key feature enabling the detection of low-abundance proteins.

The cells treated with the magnetic cell-labelling reagents are sorted within a microfluidic device sandwiched between two arrays of magnets. The cells are immunostained and visualized within the device. The number of cells and their distribution are used to generate a protein-expression profile; only one protein can be analysed per aliquot of sample (Fig. 1c). The device features eight capture zones with differing linear velocities to capture cells with varying levels of internalized MNPs (Fig. 1d and Supplementary Fig. 2). Owing to the low magnetic susceptibility of MNPs, each capture zone contains microfabricated structures to create localized regions of low flow velocity and enhanced capture dynamics (Fig. 1e). The first zone exhibits the highest linear velocity and thus retains cells with high magnetic content, because the retaining magnetic force overcomes the drag force exerted by the locally high flow velocity. The ensuing seven zones exhibit gradually reduced linear velocities (Fig. 1f). This design allows cells with high levels of the intracellular protein target to be captured in the first zone of the device, whereas cells with lower expression levels are sorted in later zones according to protein levels. It is noteworthy that the production of the device masters, a major step in the fabrication of microfluidic devices, is carried out using a stereolithographic three-dimensional (3D) printer to facilitate a large-scale production of devices for future

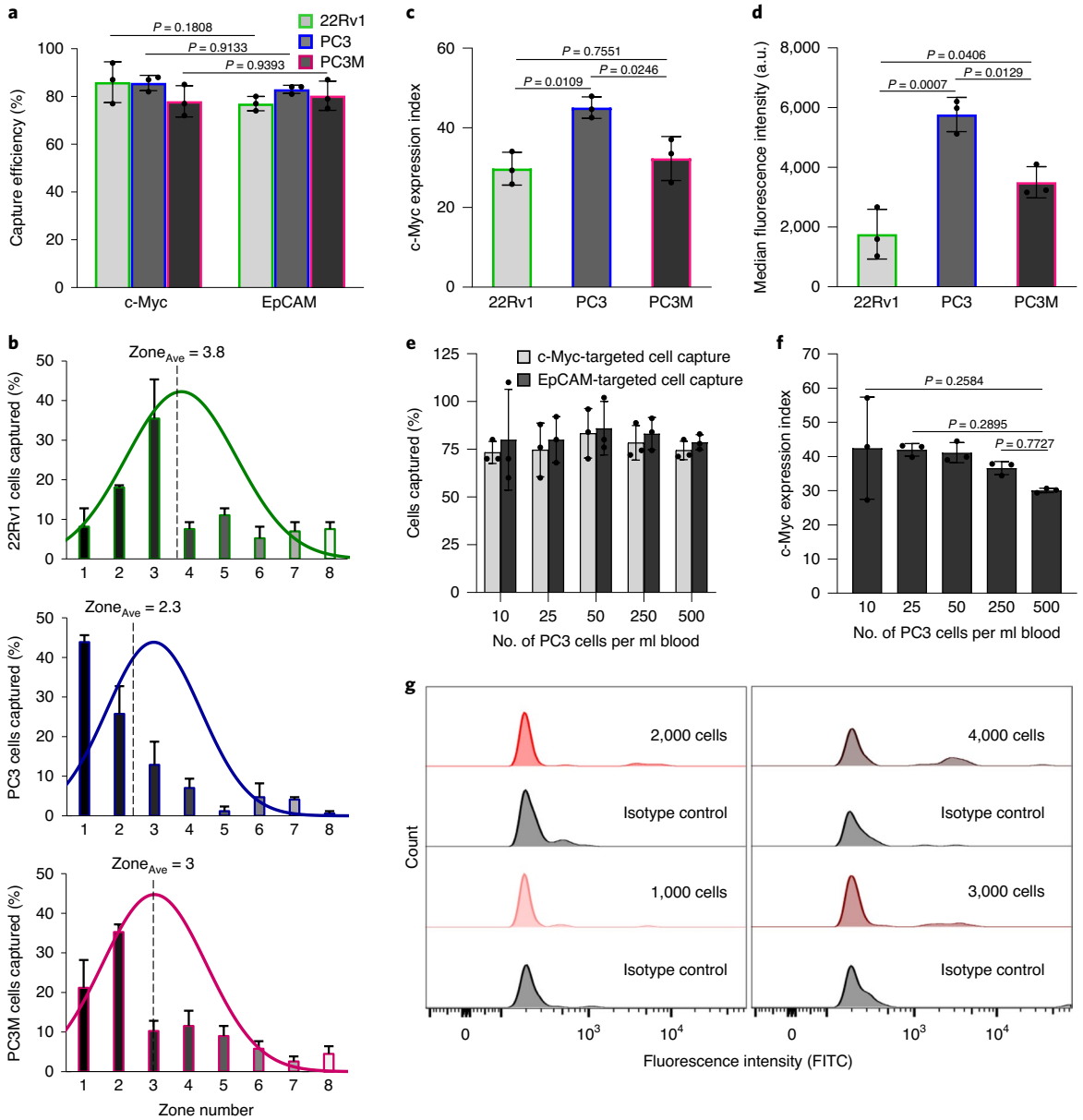

Fig. 2 | Intracellular protein analysis and the sensitivity of the approach. a, Capture efficiency of 22Rv1, PC3, and PC3M cell lines after fixation, permeabilization and incubation with a c-Myc antibody modified with ssDNAs that were subsequently hybridized with CP1 and CP2. A parallel experiment was carried out in which the cells were captured using MNPs tagged with anti-EpCAM antibody. One hundred cells were used in these trials. Data are mean ± s.d. of biological replicates ($n = 3$). The data were analysed by two-way analysis of variance (ANOVA) with Sidak's correction and 95% confidence intervals. **b**, Determination of the median capture zone ($Zone_{Ave}$) of the three cell lines. The curves represent the normal distribution fit to the data. **c**, Cellular analysis of c-Myc protein in the three cell lines. The c-Myc expression index reflects the capture of cells using the ssDNA-tagged antibody followed by hybridization with CP1 and CP2 relative to cell capture with MNP-labelled anti-EpCAM antibody. The c-Myc expression index is calculated from the formula $(N_{IP} \times 100/(N_{EpCAM} \times Zone_{Ave}))$, where N_{IP} is the number of cells captured by targeting the intracellular protein (c-Myc), N_{EpCAM} is the number of cells captured by targeting EpCAM, and $Zone_{Ave}$ is the median capture zone of the cells. **d**, Flow cytometric analysis of c-Myc protein in the three cell lines. a.u., arbitrary units. **e**, Sensitivity of the approach tested by spiking different numbers of PC3 cells into 1 ml of blood. **f**, Dynamic range of the approach determined by measuring the variation of c-Myc expression index with the number of cells spiked in a blood sample. Data are mean ± s.d. of biological replicates ($n = 3$). Data were analysed by ordinary one-way ANOVA with Tukey's correction and 95% confidence intervals. **g**, Sensitivity of the flow cytometry analysis of c-Myc in PC3 cells spiked in whole blood. A high cell count (>1,000 cells) was needed for c-Myc detection in blood after removal of RBCs using the Ficoll method. FITC, fluorescein isothiocyanate.

commercialization. In addition, we optimized the device design and flow rate and found that using X-shaped microfabricated structures (height = 50 µm, width = 200 µm) and a flow rate of 2 ml h^{-1} resulted in the highest capture efficiency (Supplementary Fig. 3). Simulations of cell capture within the device are provided in the Supplementary Information and the minimum number of beads required for cell capture was calculated for each capture zone (Supplementary Table 1). In addition, the probe sequences used in this study are provided in Supplementary Table 2.

In a first set of experiments, we assessed the efficiency of a device designed to facilitate the analysis of an intracellular protein, c-Myc, and its ability to sort cells exhibiting different levels

of the protein. The c-Myc protein is a nuclear transcription factor that regulates several cellular processes, including cell growth and proliferation, differentiation, apoptosis and motility[30]. In prostate cancer, c-Myc (nuclear and cytoplasmic) is upregulated in both androgen-receptor-positive and androgen-receptor-negative castration-resistant prostate cancers (CRPCs). In addition, c-Myc is involved in prostate cancer progression and its upregulation at either the mRNA or protein level in approximately 30% of patients is correlated with metastasis and biochemical recurrence, which can also affect the outcome of cancer radiotherapy and chemotherapy[31]. While c-Myc has been regarded as a challenging therapeutic target, recent progress is being made, with new protein therapeutics advancing to the clinic[32].

Three prostate cancer cell lines with varying phenotypic properties and c-Myc levels were used in this proof-of-concept study: 22Rv1, PC3 and PC3M[33,34]. To test the efficiency of our capture-and-analysis approach, we spiked 1 ml of healthy blood with 100 cells from each cell line and incubated the samples with single-stranded DNA (ssDNA)-labelled c-Myc antibody then hybridized the ssDNAs with MNP-conjugated capture probe (CP)1 and CP2. The cells were sorted within the microfluidic device and their sorting profiles were determined after they were immunostained for two epithelial markers, epithelial cell adhesion molecule (EpCAM) and cytokeratin, and the presence of cell nuclei was confirmed using the nuclear stain 4,6-diamidino-2-phenylindole (DAPI). Additionally, the lymphocyte antigen CD45 was immunostained to enable the identification of white blood cells. In a parallel experiment, cells suspended in blood were captured with EpCAM antibody conjugated with MNPs to gauge the overall capture efficiency and provide an overall cell or CTC count. For each of the cell lines tested, the c-Myc-mediated capture efficiencies were high (22Rv1, 86 ± 6%; PC3, 85 ± 3%; PC3M, 78 ± 5%) (Fig. 2a and Supplementary Fig. 4) and comparable with EpCAM-mediated capture efficiencies (22Rv1, 77 ± 2%; PC3, 83 ± 1%; PC3M, 83 ± 4%) (Fig. 2a and Supplementary Fig. 5).

For each cell line, the median zone of cell capture was calculated to consider the effect of intracellular protein levels on the overall cell distribution within the device and to provide a parameter that can be used to refine the calculation of protein expression. PC3 cells were mainly captured in the early zones of the device and had a median zone value of 2.3. The distribution of PC3M cells was shifted towards later zones with a median zone value of 3. The 22Rv1 cells were binned in later zones and had a median zone value of 3.8 (Fig. 2b). An expression index for the c-Myc protein was then calculated for each cell line by dividing the number of cells captured by targeting the intracellular protein by the total number of cells captured by EpCAM antibody and the median zone parameter, and multiplying this value by 100 (Fig. 2c). For example, the average number of PC3 cells captured by targeting c-Myc and EpCAM are 85 and 83, respectively; the median zone value is 2.3 and thus the expression index is 45.

Flow cytometry was used to measure the expression of c-Myc protein in the same cell lines (Fig. 2d and Supplementary Fig. 6). c-Myc expression measured using the magnetic cell-labelling approach and flow cytometry were comparable within measurement errors. The concordance of c-Myc expression index measurements and flow cytometry-based quantification supports the notion that the magnetic cell-labelling approach is quantitative. Our results also show that the c-Myc expression levels in all cell lines are low compared with the levels of the cell-surface protein EpCAM (Supplementary Fig. 7). However, similar cell-capture efficiencies were achieved by targeting c-Myc using the magnetic cell-labelling reagents and EpCAM with anti-EpCAM conjugated with MNPs (Fig. 2a). This provides further support for the ability of the method to amplify the magnetic susceptibility of cells bearing low abundance of intracellular proteins.

We next sought to determine the sensitivity and dynamic range of the magnetic cell-labelling approach. Analysis of c-Myc expression in as few as 10 cells in 1 ml of blood could be reproducibly achieved; lower cell counts could also be reliably analysed, but there were sampling errors at concentrations below 10 cells per ml. The protein expression index values were constant between 10 and 250 cells. Analysing a larger number of target cells led to saturation of the initial zones, resulting in lower expression index values (Fig. 2e,f and Supplementary Fig. 8). However, such high cell counts would not be typically encountered in most clinical specimens.

The performance of the magnetic cell-labelling approach was benchmarked against flow cytometry to assess the sensitivity of the method. PC3 cells immunostained for c-Myc and analysed by flow cytometry could be visualized at low cell counts when suspended in buffered solution. However, more than 1,000 cells, spiked in blood, were required for c-Myc analysis even after red blood cells were removed before analysis using the Ficoll method (Fig. 2g and Supplementary Fig. 9). This can be ascribed to the background signal caused by residual blood cells, which can obscure the signal emitted from the fluorescently labelled antibody.

We used this approach to analyse a series of other clinically relevant intracellular proteins in the three prostate cancer cell lines. We analysed a panel of four intracellular proteins that are present in different subcellular compartments, including cytoplasm, nucleus and mitochondria. These proteins include vimentin, poly (ADP-ribose) polymerase 1 (PARP1), octamer-binding transcription factor 4 (Oct4), and DNA-directed RNA polymerase (POLRMT). Vimentin, a cytoplasmic intermediate filament protein, is a canonical marker of epithelial–mesenchymal transition[35]. Upregulation of vimentin contributes to androgen-independent prostate cancer invasion and metastasis via Src regulation and is associated with poor survival outcomes in patients with vimentin-positive CTCs[36]. PARP1 is an abundant nuclear enzyme that is functionally involved in DNA damage repair and transcriptional regulation[37]. PARP1 interacts with the predominant TMPRSS2:ETS gene fusion product, ERG, to elicit protumorigenic effects in androgen-receptor-positive prostate cancer by transcriptionally regulating functional genes contributing to tumour growth, metastasis and resistance to therapy[38]. Oct4 is a transcription factor (nuclear and cytoplasmic) that regulates self-renewal and differentiation in embryonic stem cells, and is overexpressed in various tumours, including prostate cancer[39]. POLRMT is a single-subunit mitochondrial RNA polymerase enzyme that controls the transcription of the mitochondrial genome. POLRMT contributes functionally to tumour growth and is overexpressed in most malignancies[40].

The expression pattern of each protein was analysed using the magnetic cell-labelling approach (Supplementary Figs. 10 and 11) and the expression index values were calculated for each protein in the three cell lines (Fig. 3). Flow cytometry was used to analyse the protein levels in the same cell lines (Fig. 3 and Supplementary Fig. 12). Both methods generated comparable results, again indicating that the magnetic cell-labelling approach can be used to analyse intracellular proteins in cancer cells. It also highlights the ability of the magnetic cell-labelling reagents to reach subcellular organelles, such as nucleus and mitochondria, to facilitate the analysis of different classes of intracellular proteins. We also attempted to analyse the same proteins using antibodies directly labelled with MNPs. In these trials, the intracellular proteins were targeted with specific antibodies directly labelled with MNPs via biotin–streptavidin coupling, and the cells were sorted using the same device (Supplementary Fig. 13). Lower capture efficiencies of cells ((14 ± 3%)−(57 ± 4%)) were achieved, which prevented accurate determination of the protein levels (Supplementary Fig. 14). The results indicate that the magnetic cell-labelling reagents are crucial for the analysis of low-abundance proteins.

To demonstrate the selectivity of the approach, we analysed vimentin in PC3 cells before and after knocking down the *VIM* gene with small interfering RNAs (siRNAs). We found that the transfected PC3 cells exhibited lower expression index for vimentin, indicating a 33 ± 6.6% decrease in vimentin expression (Fig. 3e and Supplementary Fig. 15); flow cytometry analysis of vimentin revealed that the protein level decreased by 41 ± 5.9% (Fig. 3e and Supplementary Fig. 16), corroborating the protein-expression data obtained using the magnetic cell-labelling approach. In addition, fluorescence in situ hybridization (FISH) studies were carried out to determine the rate of entry of MNP-labelled capture probes into PC3 and LNCaP cells after targeting vimentin with the DNA-labelled vimentin antibody. A similar rate of entry was observed in two different cell lines with different vimentin expression levels (Supplementary Fig. 17). The results demonstrate the efficient delivery of probes enabled by this approach. Additionally, the PC3 cells captured in each zone have distinct levels of vimentin protein that increase from zone 1 to zone 8 (Supplementary Fig. 18). The increase in protein content, measured by flow cytometry, correlated with the number of magnetic beads required for cell capture in each zone. These results show that the cell capture in a particular zone is only dependant on the intracellular protein content.

We then proceeded to assess the application of this approach in samples collected from tumour-bearing animals and patients with cancer. First, we analysed the levels of c-Myc and vimentin in CTCs captured from the blood of mice bearing PC3 and PC3M orthotopic xenografts one week and three weeks after implantation. In each sample, the c-Myc and vimentin-targeted capture of CTCs was conducted along with a total cell count determined by targeting EpCAM with anti-EpCAM conjugated with MNPs. For all of the xenografted mice, substantial numbers of CTCs were detected. The CTCs collected from mice xenografted with the less metastatic PC3 cells did not show a marked upregulation of c-Myc and vimentin levels three weeks after implantation (Fig. 4a,b). Conversely, CTCs collected from animals bearing the highly metastatic PC3M-derived tumours exhibited a marked increase in c-Myc and vimentin levels after three weeks (Fig. 4c,d). Furthermore, we studied the distribution of CTCs captured by targeting c-Myc among the eight capture zones of the microfluidic device. We observed that CTCs obtained from the PC3M xenograft were captured mainly in earlier zones, whereas CTCs collected from the PC3 xenograft were sorted in later zones. This indicates a higher level of c-Myc in CTCs collected from the PC3M xenograft compared to those collected from the PC3 xenograft (Fig. 4e). A similar cell distribution pattern was observed for vimentin-targeted capture of CTCs obtained for both xenografts, indicating a higher vimentin level in CTCs obtained from the PC3M xenograft (Fig. 4f). We found a strong correlation between the mRNA expression level (Supplementary Figs. 19–21) and the protein abundance previously demonstrated in Figs. 2c and 3a, with Pearson's $r = -0.94$ and -0.99 for c-Myc and vimentin, respectively. The results agree with previous reports that demonstrated a similar correlation between the expression levels of c-Myc[41] and vimentin mRNAs[42] and the abundance of the corresponding proteins in prostate cancer.

To demonstrate the clinical utility of the approach, we conducted a study in which we measured the levels of c-Myc and vimentin in CTCs captured from blood samples collected from a small cohort of

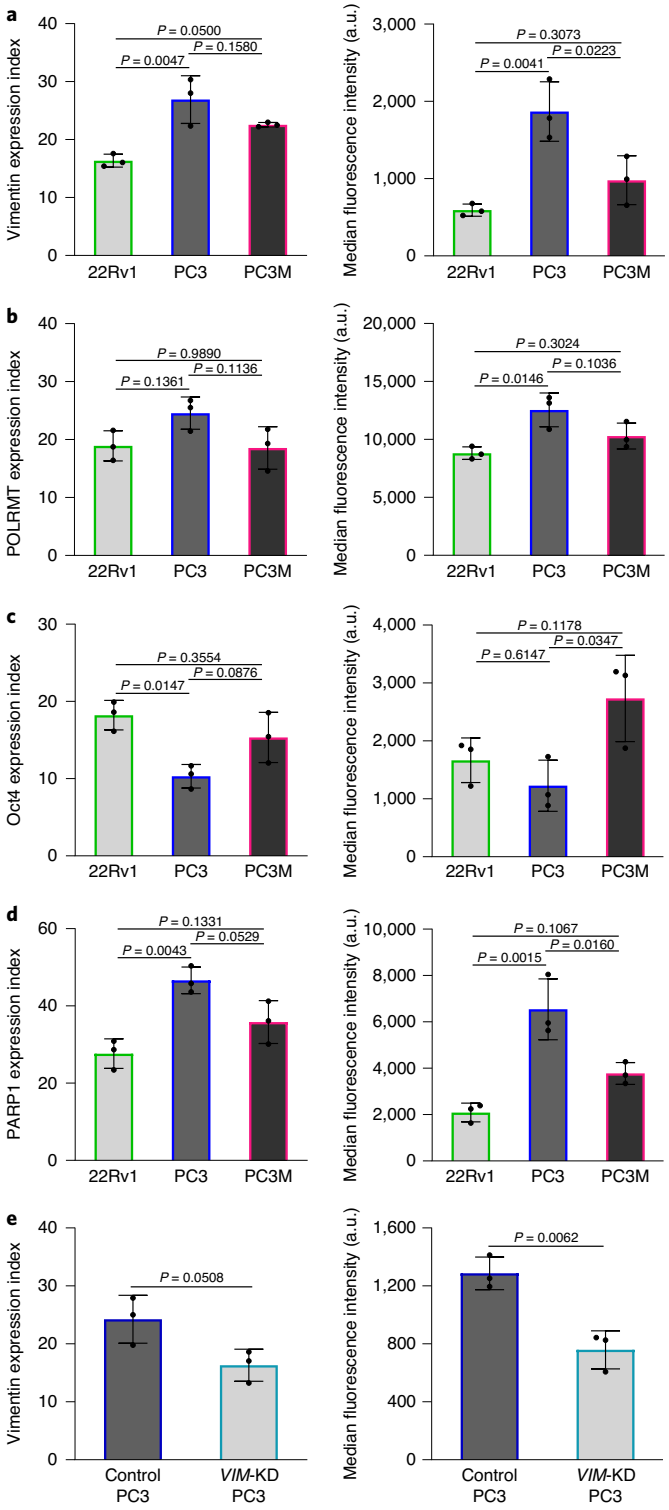

Fig. 3 | Analysis of clinically relevant intracellular proteins. a–d, Cellular analysis of four intracellular proteins, including vimentin (**a**), POLRMT (**b**), Oct4 (**c**) and PARP1 (**d**), in three prostate cancer cell lines using the single-cell approach (left graphs) and flow cytometry (right graphs). A total of 100 cells and 100,000 cells were used for the single-cell analysis and flow cytometry trials, respectively. The agreement between the intracellular protein-expression indices determined using the single-cell approach and flow cytometry indicates that the method is quantitative. Data are mean ± s.d. of biological replicates ($n = 3$). Data were analysed by ordinary one-way ANOVA with Turkey's correction and 95% confidence intervals. **e**, Analysis of vimentin in PC3 cells after knocking down the *VIM* gene using the single-cell approach (left) and flow cytometry (right). Data are mean ± s.d. of biological replicates ($n = 3$). Data were analysed by unpaired two-tailed Student's *t*-test.

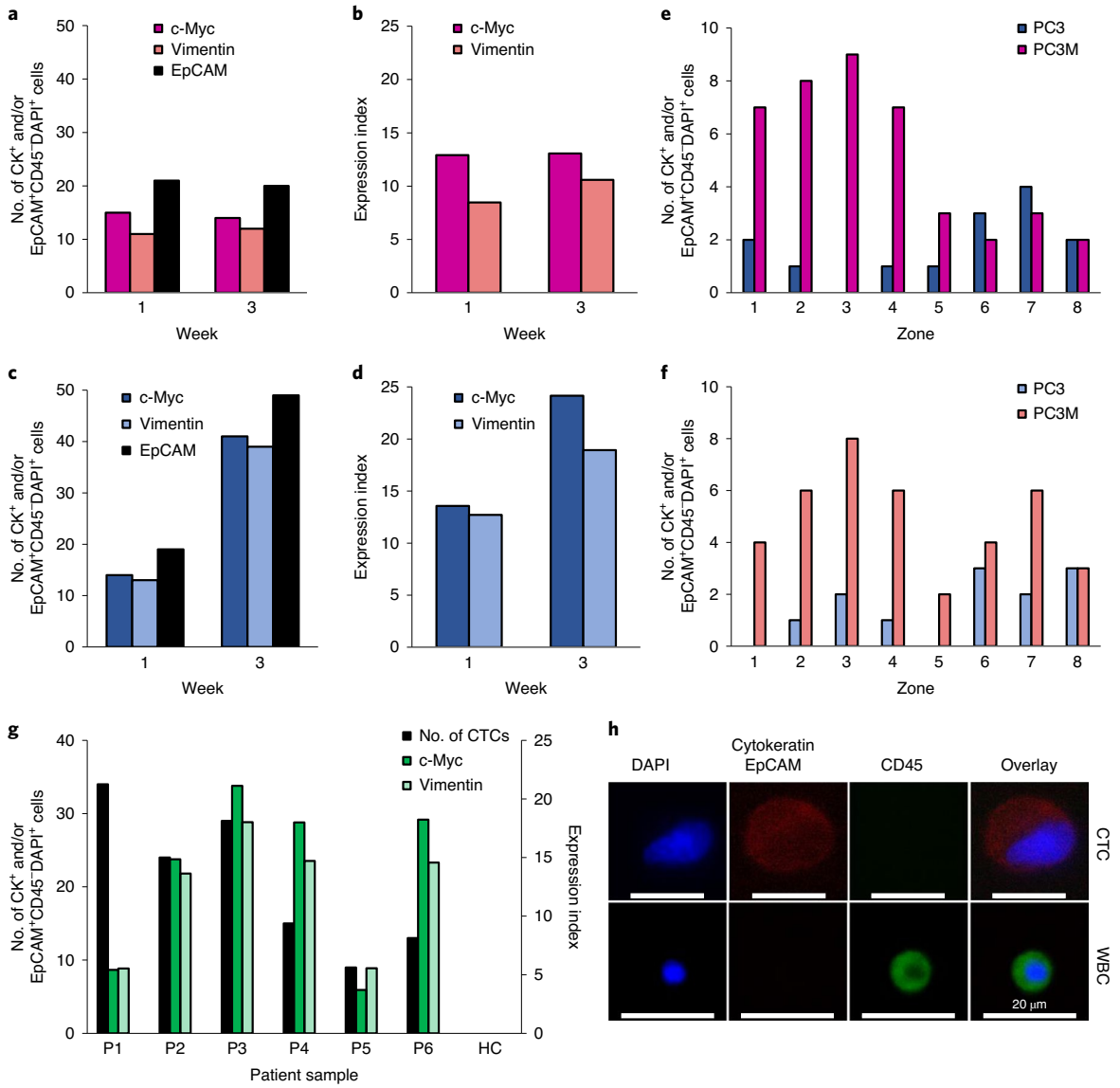

Fig. 4 | Analysis of c-Myc and vimentin in xenografts and clinical samples. a, Number of CTCs captured from the blood of mice 1 and 3 weeks after implantation of PC3 cells. CTCs were captured by targeting c-Myc, vimentin and EpCAM after removal of RBCs using the Ficoll method. CK, cytokeratin. **b**, Single-cell analysis of c-Myc and vimentin expression at the corresponding time points. **c**, Number of CTCs captured from the blood of mice bearing PC3M xenografts after 1 and 3 weeks. **d**, Single-cell analysis of c-Myc and vimentin expression at the corresponding time points. **e**,**f**, Number of CTCs captured from the blood of mice bearing PC3M and PC3 xenografts after 3 weeks by targeting c-Myc (**e**) or vimentin (**f**). **g**, Single-cell analysis of c-Myc and vimentin expression in the CTCs collectively isolated from the blood samples of a cohort of six patients with prostate cancer (P1–P6) and one healthy control (HC). **h**, Representative image of a CTC captured from a blood sample from a patient with prostate cancer, compared with a white blood cell (WBC). A single image was acquired for each cell type. The cells were stained with APC-labelled anti-cytokeratin, APC-labelled anti-EpCAM, Alexa Fluor 488-labelled anti-CD45 and DAPI. Only cytokeratin$^+$ and/or EpCAM$^+$CD45$^-$DAPI$^+$ cells were counted as CTCs.

patients undergoing treatment for metastatic CRPC. An average of 10 ml of blood was analysed per patient and CTCs were identified using immunofluorescence. In four of the six patients tested, high levels of c-Myc and vimentin were detected in the CTCs isolated from blood (Fig. 4g). Representative images of a CTC captured from patient samples versus a white blood cell are shown in Fig. 4h. The quantitative PCR data revealed that the same four patients exhibited high levels of c-Myc mRNA expression ($r = -0.81$). However, a discrepancy was noted between the vimentin mRNA expression and the protein abundance ($r = -0.69$) (Supplementary Fig. 22).

Unlike conventional tumour markers that are simply associated with tumours, genetically altered oncoproteins are produced only by tumour cells and are responsible for the initiation or progression of tumours[43]. Proteins harbouring tumour-specific mutations or fusions are targeted by tumour therapeutics[43]. However, before these therapeutics can be administered, it is critical that patients are assessed to determine whether their tumours show perturbations in specific molecular targets. While immunohistochemistry performed on biopsy specimens is a key tool for this type of analysis, disease found in metastatic cancer patients may not be accurately represented in a biopsy of a primary tumour, and an initial biopsy taken during diagnosis may not reflect the molecular changes that occur over the course of a patient's treatment. Assessing drug targets via liquid biopsy, however, provides a means to profile the

molecular markers present in primary and metastatic tumours at any time point required for therapeutic selection. We therefore sought to apply our magnetic cell-labelling approach to a panel of intracellular protein markers that are validated targets of anticancer therapy. These proteins represent classes of oncogenic proteins that can arise from either gene splicing, gene fusion or gene mutation.

Androgen-deprivation drugs are commonly used to treat advanced prostate cancer; these drugs, which include abiraterone and enzalutamide[44], either suppress the synthesis of extragonadal androgens or target the androgen receptor directly. Approximately 20–40% of patients show no response to androgen-deprivation therapy (ADT), whereas those who initially have a response to ADT acquire a secondary resistance and thus require a second-line chemotherapy (for example, docetaxel)[45]. One plausible explanation for resistance to ADT may involve the presence of splice variants of androgen receptor genes that encode for a truncated androgen receptor protein. The androgen receptor splice variant 7 (ARV7) is the most abundantly expressed variant and has been recently identified as a predictive biomarker for ADT[46]. Using our magnetic cell-labelling approach, we were able to detect this splice variant in blood containing ARV7-positive cells. A negligible expression index was measured for a blood sample containing ARV7-negative cells (Fig. 5a and Supplementary Fig. 23).

Next, we analysed other abnormal oncoproteins resulting from gene fusions. *NTRK* gene fusions cause overexpression of the transmembrane tropomyosin receptor kinase receptors referred to as TrkA, TrkB and TrkC. Treatment of *NTRK* fusion-positive patients with Trk inhibitors, such as larotrectinib or entrectinib, is associated with high response rates (more than 75%), regardless of the tumour histology[47]. This finding has led to 'basket' clinical trials in which patients are enrolled on the basis of *NTRK* fusion status rather than tumour type. The detection of *NTRK* fusions using sequencing-based analysis is challenging, however, because of the presence of large introns[48]. Therefore, identifying gene fusions as expressed proteins is advantageous. The results shown in Fig. 5a indicate that we are able to detect TrkB in blood samples spiked with lung cancer cells positive for the protein fusion. A lower expression index was measured for TrkB in samples containing myelogenous leukaemia cells (Supplementary Fig. 23). While the expression index values measured for non-target cells were consistently low, it is notable that statistical tests indicate that the variability in these measurements diminished the statistical significance attained with this target.

In chronic myeloid leukaemia (CML), pathogenesis involves the fusion of the breakpoint cluster region (*BCR*) on chromosome 22 with the Abelson murine leukaemia (*ABL1*) gene on chromosome 9, resulting in the formation of a fusion hybrid gene that encodes a cytoplasmic BCR–ABL1 oncoprotein with tyrosine kinase activity. The US Food and Drug Administration (FDA)-approved tyrosine kinase inhibitors for treatment of CML, such as nilotinib, imatinib, bosutinib and dasatinib, have improved the overall survival rate of patients with CML[49]. The magnetic cell-labelling approach enabled detection of the mutant protein in samples containing BCR–ABL1-positive leukaemia cells (Fig. 5a). A negligible expression index was measured for BCR–ABL1 in control samples containing T-lymphocyte cells (Supplementary Fig. 23).

We also analysed abnormal oncoproteins resulting from gene mutations. Most *BRAF* mutations commonly found in patients with melanoma and colorectal cancer result in an amino acid change of valine to glutamate in the nuclear and cytoplasmic protein, resulting in BRAF(V600E). The BRAF(V600E) mutation causes constitutive activation of the MAP kinase pathway, leading to drug and immune resistance, apoptosis evasion and cancer metastasis[50]. BRAF(V600E)-positive tumours can be controlled with FDA-approved BRAF inhibitors, such as vemurafenib and dabrafenib[51]. Our approach enabled detection of the mutated protein in blood samples containing BRAF(V600E)-positive colon cancer cells. A negligible expression index was measured for samples containing BRAF(V600E)-negative prostate cancer cells (Fig. 5a and Supplementary Fig. 23).

Another mutated protein that is an important marker in breast and prostate cancer is BRCA2. Patients with breast cancer with mutations in the *BRCA2* gene are more susceptible to recurrence of breast cancer or development of ovarian cancer[52]. Most cancer-associated BRCA2 protein mutations are C-terminal-truncating mutations that cause the protein to accumulate in the cytoplasm[53]. In 2018, the FDA approved a PARP inhibitor (olaparib) for the treatment of advanced breast and ovarian cancer with BRCA mutations[54], and clinical evidence is mounting that the drug is also effective in patients with prostate cancer harbouring BRCA2 truncations[55]. It is therefore critical to develop liquid-biopsy tests for this mutated protein that can be used for therapeutic selection. The structures of wild-type and mutated BRCA2 proteins are depicted schematically in Fig. 5b. Blood samples were spiked with Capan1 cells and analysed for the truncated BRCA2 protein, and the cell-capture results were compared those obtained using Panc1 cells expressing wild-type BRCA2. Unlike BRAF(V600E) protein, there is no antibody specific for the truncated BRCA2 protein. Thus, cells were immunostained and counted subsequent to targeting the N terminus of BRCA2, the C terminus of BRCA2 and EpCAM (Fig. 5c and Supplementary Fig. 23). The results demonstrate the ability of the approach to detect mutated BRCA2 protein in blood samples spiked with a small number of cells, with minimal interference from wild-type BRCA2 protein (Fig. 5d). Furthermore, all protein analysis results obtained using the magnetic cell-labelling approach corroborated the flow cytometry data within the margin of error (Supplementary Figs. 24 and 25). We also used this approach for parallelized analysis of eight intracellular proteins, including c-Myc, vimentin, Oct4, ARV7, BRCA2, TrkA, KRAS 2B and cytokeratin in healthy blood samples spiked with MDA-MB-231 cells (Supplementary Fig. 26 and 27); the results corroborated the flow cytometry data ($r = 0.83$) (Supplementary Fig. 28).

Finally, we set out to assess the utility of the approach for predicting the response of tumours to a molecular-targeted therapy. BRCA2 mutations are common in tumours and lead to impaired homology-directed DNA repair, making these tumours sensitive to therapeutic agents that target homology-directed DNA repair, such as PARP inhibitors[56]. We conducted a study in which we measured the level of mutated BRCA2 protein in CTCs captured from the blood of mice bearing either Capan1 or Panc1 xenografts, as representatives of BRCA2-deficient and BRCA2-proficient tumours, respectively. At day seven after implantation, the tumour-bearing mice were divided into control and treatment groups. Mice in the treatment groups received olaparib, whereas the control groups received the vehicle (Fig. 5e). In each sample, the C terminus and N terminus of BRCA2-targeted capture of CTCs were conducted along with a total cell count determined by targeting EpCAM with anti-EpCAM conjugated with MNPs. For all of the xenografted mice, substantial numbers of CTCs were detected. The CTCs collected from mice xenografted with Capan1 cells exhibited detectable levels of mutated BRCA2 protein at day 7, 22 and 37 after implantations, whereas CTCs from Panc1-xenografted mice did not exhibit similar levels of the mutated BRCA2 protein (Fig. 5f and Supplementary Figs. 29 and 30). Monitoring the tumour growth in mice demonstrated that treatment with olaparib resulted in a marked inhibition of tumour growth in Capan1-xenografted mice, whereas Panc1-xenografted mice were not affected (Fig. 5g,h). The results validate the utility of the approach for predicting the therapeutic response of susceptible and resistant tumours in vivo and present a use case for how this technology could be used in the clinic.

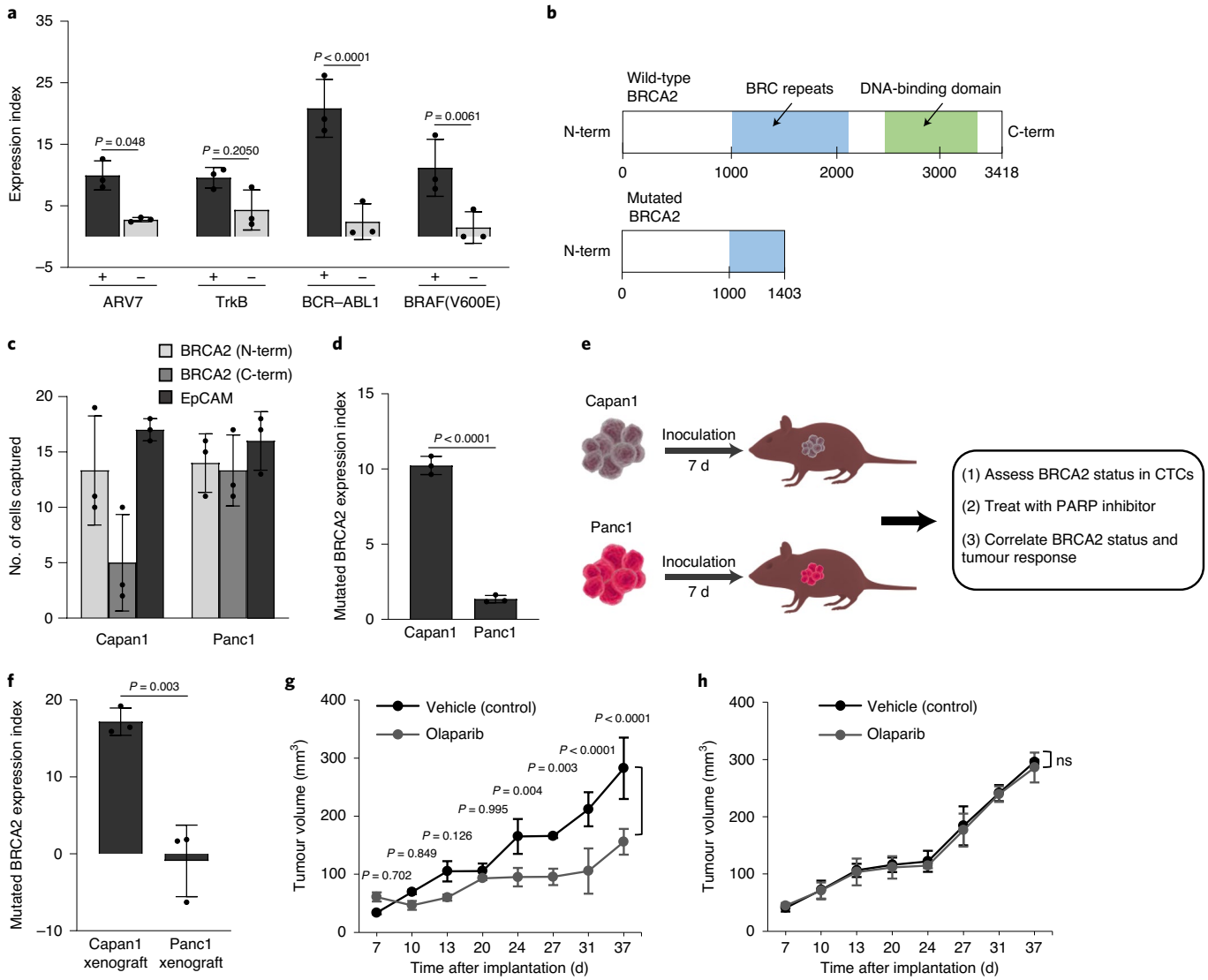

Fig. 5 | Analysis of mutated proteins relevant for therapeutic selection. a, Analysis of ARV7 in 22Rv1 (+) and LNCaP (−) cells (30 cells per ml blood), TrkB in H460 (+) and K562 (−) cells (30 cells per ml PBS), BCR–ABL1 in K562 (+) and Jurkat cells (−) (30 cells per ml PBS), and BRAF(V600E) in HT29 (+) and DU145 (−) cells (30 cells per ml blood). After removal of RBCs, cell fixation and permeabilization, cells were captured by targeting the intracellular protein. A parallel experiment was carried out in which cells were captured by targeting either EpCAM or CD45 (for K562 and Jurkat cells). Samples that tested positive for the proteins in flow cytometry assays exhibited higher expression indices than those that tested negative. **b**, Graphical representation of the structures of wild-type and mutated (truncated) BRCA2 proteins. N-term, N terminus; C-term, C terminus. **c**, Analysis of mutated BRCA2 protein in 1 ml blood samples spiked with Capan1 or Panc1 cells (30 cells). Cells were captured by targeting mutated BRCA2 protein with N-terminus-specific antibody and C-terminus-specific antibody and are compared with the number of cells captured with anti-EpCAM. **d**, Samples that tested positive for mutated BRCA2 protein in flow cytometry assays exhibited higher expression indices than those that tested negative. **e**, Schematic illustration for therapeutic protein analysis in xenografted mice. **f**, Analysis of mutated BRCA2 protein in CTCs captured from the blood of mice bearing either Capan1 or Panc1 xenograft. The analysis was carried out at day 7 after tumour formation. An extended analysis is provided in Supplementary Fig. 30. After tumour formation, the mice were randomly divided into control and treated groups ($n = 3$). Mice in the treated group received 50 mg kg^{-1} olaparib every other day. Mice in the control group received only the vehicle. **g**–**h**, Tumour volume is plotted against duration of treatment for Capan1 (**g**) and Panc1 (**h**) xenografts. Data are mean ± s.d. of biological replicates ($n = 3$). Data were analysed by two-way ANOVA (**a**,**g**,**h**) with Holm–Sidak test for multiple comparisons and 95% confidence intervals, or unpaired two-tailed Student's *t*-test (**d**,**f**).

Outlook

The method reported here enables direct isolation of rare CTCs from blood and intracellular protein analysis in a single experiment. This approach is quantitative when benchmarked against flow cytometry and can be used to analyse small (around 10) numbers of cells. The analytical performance of the approach is benchmarked against FACS-based microfluidic western blotting in Supplementary Table 3. The precision and detection sensitivity with low cell counts obviates the need for post-isolation cell culture. The approach relies on immunostaining for identification of target cells and is thus not susceptible to interference from residual blood cells. Moreover, it does not require any enzymatic amplification steps. It is notable that EpCAM-based CTC capture is used to provide an overall count of CTCs relative to those captured using specific markers targeted for quantification, but given the ability to use any antibody with the method, a mixture of antibodies can be used to generate the overall CTC count.

Furthermore, the method can be used for parallelized analysis of a panel of protein markers in CTCs—a capability particularly beneficial for studying tumour metastasis pathways that usually involve cascades of several proteins. Combining CTC isolation with protein profiling would improve CTC taxonomy, as some CTCs do not resemble the primary tumour and probably diverge at the proteomic level. Given the inherent long-term solution-phase storage stability of antibody–DNA conjugates, we foresee that the magnetic cell-labelling reagents will continue to provide a useful tool for evaluation of subcellular proteins. More broadly, we envision the role of the magnetic cell-labelling approach as a useful tool with relevance spanning from understanding CTC biology, early cancer detection and monitoring patients' response to particular therapeutic regimens.

Methods

Device fabrication. Devices were fabricated using a standard soft-lithography procedure. Masters were fabricated by a stereolithographic 3D printer (μMicrofluidics Edition 3D Printer, Creative CADworks) according to the manufacturer's protocol. Polydimethylsiloxane (PDMS, Dow Chemical, US) replicas were poured on masters and baked at 70 °C for 2 h. The cured replicas were then peeled off, punched, and plasma bonded to thickness no. 1 glass coverslips (Ted Pella). The bonded chips were kept at 100 °C overnight to secure a robust bonding. Afterwards, the silicon tubing was attached to the inlet and outlet of the device. Before use, the devices were conditioned with 1% Pluronic F68 (Sigma-Aldrich) in phosphate buffered saline (PBS) for at least 4 h to reduce the nonspecific adsorption. Each device was sandwiched between two arrays of N52 Nd FeB magnets (K&J Magnetics; 1.5 mm by 8 mm) with alternating polarity. A syringe pump (Chemyx) was used during the cell-capture process.

Cell culture. PC3M, 22Rv1, LNCaP, H460 and Jurkat cell lines were cultured in RPMI-1640 medium (ATCC 30-2001). The PC3 cell line was cultured in F-12K medium (ATCC 30-2004). The DU145 cell line was cultured in EMEM medium (ATCC 30-2003). The MDA-MB-231 cell line was cultured in L-15 medium (ATCC 30-2008). The HT29 cell line was cultured in McCoy's 5A medium (ATCC 30-2007). The Panc1 cell line was cultured in Dulbecco's modified Eagle's medium (ATCC 30-2002). The Capan1 and K562 cell lines were cultured in IMDM medium (ATCC 30-2005). All media were supplemented with 10% FBS (20% FBS for Capan1 cell culture in IMDM) and 1% penicillin–streptomycin and the cells were cultured at 37 °C and 5% CO_2 in T75 flasks. Cells were harvested when they reached more than 70–80% confluence. With the exception of K562 and Jurkat cell lines, cells were detached from the culture dishes using 1 ml of 0.25% (w/v) trypsin–0.53 mM EDTA solution for 3 min at 37 °C. The cells were then filtered using a 40 μm BD falcon cell strainer (Becton, Dickinson).

Preparation of DNA-conjugated antibodies. Fourteen antibodies, including antibodies specific to c-Myc (bs-4963R, Bioss), vimentin (bs-0756R, Bioss), Oct4 (bs-1111R, Bioss), POLRMT (489004 Pab, USBiological), PARP1 (LS-C745005, LifeSpan Biosciences), ARV7 splice variant antibody (31-1109-00, RevMAb Biosciences), BCR–ABL1 (ab187831, Abcam), BRAFv600E (31-1042-00, RevMAb Biosciences), TrkA (ab76291, Abcam), TrkB (ab134155, Abcam), BRCA2 (N-terminus specific, ab75335, Abcam) and BRCA2 (C-terminus specific, ARG10523, Arigo Biolaboratories), pan cytokeratin (bs-1712R, Bioss) and KRAS 2B (16155-1-AP, Proteintech) were first modified with streptavidin using a streptavidin-conjugation kit (Abcam) according to the manufacturer's protocol. In brief, 100 μl of the antibody solution (1 mg ml^{-1}) was gently shaken with 10 μl of the activator. Subsequently, the activated antibodies were incubated with 33 μg streptavidin overnight at 4 °C. Next, 10 μl of the quencher was added to stop the reaction. Then, 80 μl of the biotin-labelled DNA (1 mg ml^{-1}) was added and the mixture was incubated at room temperature for 30 min. Finally, the solution was stored at 4 °C until use.

Preparation of capture probes. In brief, 100 μl of 20 μM antisense oligonucleotide solution in Dulbecco's PBS (DPBS, Sigma-Aldrich) containing 1 mM dithiothreitol (DTT, Sigma-Aldrich), were heated for 5 min at 60 °C for deaggregation. Afterwards, the solution was transferred to a microtitre plate and incubated with 1.5 μl of 10 mg ml^{-1} streptavidin-coated MNPs (100 nm, Chemicell) for 30 min at room temperature. Subsequently, the MNP-labelled capture probe (CP1 or CP2) was pelleted using a magnetic-ring stand (Thermofisher Scientific) and washed three times with DPBS/DTT solution.

Intracellular protein analysis. Prostate cancer cell lines (100 cells in 100 μl DPBS containing 0.2 mg ml^{-1} dextran sulfate) were fixed with 100 μl of 8% paraformaldehyde (PFA, Sigma-Aldrich) solution in DPBS/DTT for 15 min at 37 °C. After centrifugation, the cells were incubated with 100 μl of 0.3% Triton X-100 (Sigma-Aldrich) in DPBS/DTT for 10 min at room temperature. The cells were then gently shaken with 5 μl DNA-conjugated antibody for 30 min at room temperature. After centrifugation, the cells were gently shaken with a mixture of CP1 and CP2 (100 μl each in DPBS/DTT) for 3 h at room temperature. In parallel, 100 cells in 100 μl DPBS were gently shaken with 20 μl of MNP-labelled EpCAM antibody (130-061-101, Miltenyi Biotec) for 30 min at room temperature. Finally, the cells were loaded into the microfluidic device at a flow rate of 2 ml h^{-1}.

Cell staining and imaging. Captured cells were counted using a fluorescence microscope. Before staining, captured cells were fixed inside the device with 100 μl of 4% PFA in DPBS/DTT then permeabilized with 100 μl of 0.2% Triton X-100 in DPBS/DTT. Captured cells were immunostained with a mixture of 3% allophycocyanin (APC)-labelled pan cytokeratin antibody (GTX80205, Genetex), 3% APC-labelled EpCAM antibody (APC–EpCAM, 130-111-000, Miltenyi Biotec) and 3% Alexa Fluor 488-labelled CD45 antibody (AF488-CD45, MHCD4520, Invitrogen) in 200 μl PBS containing 1% bovine serum albumin (BSA, Sigma-Aldrich) and 0.1% Tween-20 (Sigma-Aldrich). Immunostaining was carried out for 60 min at a flow rate of 200 μl h^{-1}. After washing with 0.1% Tween-20 in PBS, the cells were stained with 1 drop of DAPI Prolong Gold nuclear stain (Invitrogen) in 200 μl PBS for 10 min at a flow rate of 1,200 μl h^{-1}. After staining, the cells were washed with 0.1% Tween-20 in PBS and stored at 4 °C. Finally, chips were scanned using a Nikon Ti-E Eclipse microscope with an automated stage controller and CMOS Camera (Andor Neo). The blue channel was used for DAPI staining, with a typical exposure time of 10–20 ms. The green channel was used for the Alexa Fluor 488–CD45 staining, with a typical exposure time of 40–60 ms. The red channel was used for the APC–cytokeratin and APC–EpCAM staining, with a typical exposure time of 200–300 ms. The exposure time was set individually for each chip and kept constant in the course of scanning. Cells were counted by overlaying the bright field and red, blue and green fluorescent images.

Calculation of expression index. The intracellular protein-expression index is calculated from equation (1):

$$\text{Intracellular protein expression index} = (N_{IP} \times 100)/(N_{Ab} \times \text{Zone}_{Ave}) \quad (1)$$

N_{IP} denotes the number of cancer cells captured by targeting the intracellular protein, N_{Ab} is the total number of cells in the sample captured by targeting EpCAM, and Zone_{Ave} is the median capture zone determined from a normal distribution fit to the distribution of cell populations bearing varying expression levels of the target intracellular protein.

The BRCA2 truncated (mutated) protein-expression index is calculated from equation (2):

$$\text{Intracellular truncated protein expression index} = \left[\left(N_{ITP(Nterminus)} \times 100\right)/\left(N_{Ab} \times \text{Zone}_{Ave(Nterminus)}\right) - \left(N_{ITP(Cterminus)} \times 100\right)/\left(N_{Ab} \times \text{Zone}_{Ave(Cterminus)}\right)\right] \quad (2)$$

$N_{ITP(Nterminus)}$ denotes the number of cancer cells captured by targeting the N terminus of the intracellular truncated protein, $N_{ITP(Cterminus)}$ represents the number of cancer cells captured by targeting the C terminus of the truncated protein, N_{Ab} is the total number of cells in the sample captured by targeting EpCAM, and $\text{Zone}_{Ave(Nterminus)}$ and $\text{Zone}_{Ave(Cterminus)}$ represent the median capture zones determined from a normal distribution fit to the distribution of cell populations calculated after targeting the N terminus and C terminus of intracellular truncated protein, respectively.

Dynamic light scattering. Dynamic light scattering experiments were carried out using a Zeta sizer Nano series (Malvern Instruments) to confirm the formation of MNP aggregates upon hybridization between CP1, CP2 and the ssDNA conjugate of c-Myc antibody. Before the analysis, CP1 and CP2, each composed of 15 μg MNPs modified with antisense oligonucleotide, were incubated with 5 μl DNA-conjugated c-Myc antibody for 3 h at room temperature. A control experiment was carried out in which 30 μg MNPs were incubated directly with 10 μl of 100 μg ml^{-1} biotin-labelled c-Myc antibody (bs-0842R-Biotin, Bioss) for 3 h at room temperature.

Flow cytometric analysis of proteins. Flow cytometry was used to analyse the levels of c-Myc, vimentin, POLRMT, Oct4 and PARP1 in 22Rv1, PC3M and PC3 cell lines. In brief, PC3 cells (100,000 cells) were incubated with the blocking buffer (2% BSA in PBS) for 30 min on ice. Then, the cells were fixed with 4% PFA and permeabilized with 0.2% Triton X-100. The cells were incubated with 10 μl of 100 μg ml^{-1} c-Myc antibody (bs-4963R, Bioss), vimentin antibody (bs-0756R, Bioss), Oct4 antibody (bs-1111R, Bioss), POLRMT antibody (489004 Pab, USBiological), PARP1 antibody (LS-C745005, LifeSpan Biosciences) for 30 min at room temperature. Control experiments were carried out in which the cells were incubated with 10 μl of 100 μg ml^{-1} of rabbit IgG isotype control (02-6102, Invitrogen) for 30 min at room temperature. After washing, the cells

were incubated with 10 µl of FITC-labelled mouse anti-rabbit antibody (31584, Invitrogen) for 30 min at room temperature. In addition, flow cytometry was used to analyse the levels of ARV7 in 22Rv1 and LNCaP cell lines, BCR–ABL1 in K562 and Jurkat cell lines, BRAF(v600E) in HT29 and DU145 cell lines, TrkB in H460 and K562 cell lines, and truncated BRCA2 in Capan1 and Panc1 cell lines. In these trials, the fixed and permeabilized cells were incubated with 10 µl of 100 µg ml^{-1} of ARV7 splice variant antibody (31-1109-00, RevMAb Biosciences), BCR–ABL1 antibody (ab187831, Abcam), BRAFv600E (31-1042-00, RevMAb Biosciences), TrkA antibody (ab76291, Abcam), TrkB antibody (ab134155, Abcam), BRCA2 (N-terminus specific, ab75335, Abcam), BRCA2 (C-terminus specific, ARG10523, Arigo Biolaboratories), pan cytokeratin antibody (bs-1712R, Bioss), and KRAS 2B antibody (16155-1-AP, Proteintech) for 30 min at room temperature. Control experiments were carried out in which the cells were incubated with 10 µl of 100 µg ml^{-1} of rabbit IgG isotype control (02-6102, Invitrogen) for 30 min at room temperature. After washing, the cells were incubated with 10 µl of APC-labelled anti-rabbit IgG (F0111, R&D Biosystems) for 30 min at room temperature. For BCR–ABL1 analysis, the cells were incubated with 10 µl of APC-labelled anti-mouse IgG (F0101B, R&D Biosystems) for 30 min at room temperature. Control experiments were carried out in which the cells were incubated with 10 µl of 100 µg ml^{-1} of mouse IgG isotype control (10400C, Invitrogen) for 30 min at room temperature. After washing, the cells were incubated with 10 µl of APC-labelled anti-mouse IgG (F0101B, R&D Biosystems) for 30 min at room temperature. Prior to analysis, the cells were washed three times with 2% BSA in PBS. Finally, samples were injected into a FACSCanto flow cytometer (BD Biosciences) and measurements were plotted as histograms. Absorbance values were normalized to unstained control. A total of 10,000 cells were analysed per cell line.

Knockdown of vimentin. We used *VIM*-specific Accel smart pool siRNA to knock down vimentin in PC3 cells, according to the manufacturer's protocol. In brief, PC3 (100,000 cells) were cultured at 37 °C and 5% CO_2 in a six-well plate overnight. A stock solution of 100 µM *VIM*-specific Accel smart pool siRNA (E-0003551-00-0020, Dharmacon) in 1× siRNA buffer (B-002000-UB-100) was prepared. The siRNA was suspended in 300 µl Accel delivery medium (B-005000-500, Dharmacon) to a final concentration of 1 µM and the suspension was shaken for 90 min at room temperature. The suspension was centrifuged briefly. The culture medium was aspired from each well and the cells were incubated with 300 µl siRNA suspension in the Accel delivery medium for 96 h at 37 °C and 5% CO_2. A control experiment was carried out in which the cells were incubated with 1 µM non-targeting siRNA (D-001206-13-20, Dharmacon) in the Accel Delivery medium (300 µl) under the same conditions. Finally, the cells were trypsinized and the vimentin protein level was analysed using the microfluidic approach and flow cytometry.

Quantitative PCR with reverse transcription. Total RNA was isolated from the cells using a single-cell RNA purification kit (51800, Norgen Biotek) according to the manufacturer's protocol. The isolated RNA was used for cDNA synthesis using SuperScript III first-strand synthesis system (Invitrogen), which contains random hexamer primers and Superscript III reverse transcriptase, according to the manufacturer's protocol. A comparative C_t experiment was performed on ABI 7500 real-time PCR system (Applied Biosystems). The assay was carried out in triplicates using 10 ng cDNA for each sample in a 96-well plate. The 20 µl reaction mix consisted of 10 µl of SsoFast EvaGreen master mix (Bio-Rad), 0.5 µl of forward primer (10 µM), 0.5 µl of reverse primer (10 µM), 8 µl of water and 1 µl of 10 ng µl^{-1} cDNA. Cycling conditions for the quantitative PCR were 95 °C for 10 min, followed by 40 cycles of 95 °C for 15 s and 60 °C for 1 min.

Prostate cancer xenografts. All animal experiments were carried out in accordance with the protocol approved by the University of Toronto Animal Care Committee. Male athymic nude mice (6–8 weeks old) were purchased from Envigo and maintained at the University of Toronto animal facility. Tumour xenografts were generated by injecting a suspension of 1×10^6 PC3M or PC3 cells in 25 µl Hank's buffered salt solution (Life Technologies) orthotopically into the right dorsolateral lobe of the prostate. The whole blood was collected every week from each mouse by cardiac puncture under anaesthesia. All blood samples were collected in BD vacutainer blood collection tubes containing EDTA (BD Biosciences). A total of 5 ml whole blood was collected from 5 mice after 1 and 3 weeks. The mononuclear cells were isolated using the Ficoll method and subsequently suspended in 1 ml of DPBS/DTT. In brief, the blood sample was diluted with an equal volume of PBS containing 2% FBS. The density gradient medium was added to the SepMate tube (StemCell Technologies) by pipetting through the central hole of the insert. The sample was centrifuged at 1,200*g* for 10 min at room temperature. The top layer containing the enriched mononuclear cells was poured into a new tube and washed 2 times with PBS containing 2% FBS. Each time, the sample was centrifuged at 300*g* for 8 min. For intracellular protein analysis, 200 µl of the supernatant were incubated with 200 µl of 8% PFA in DPBS/DTT for 15 min at 37 °C. After centrifugation, the cells were incubated with 100 µl of 0.3% Triton X-100 in DPBS/DTT for 10 min at room temperature. Afterward, the cells were gently shaken with 5 µl of the DNA-conjugated antibody (specific for c-Myc or vimentin) for 30 min at room temperature. After centrifugation, the cells were gently shaken with a mixture of CP1 and CP2 in DPBS/DTT (100 µl each) for 3 h at room temperature. To determine the total number of cells in the sample, 200 µl of the supernatant was incubated with 20 µl of MNP-labelled EpCAM antibody for 30 min at room temperature. The cells were loaded into the microfluidic device at a flow rate of 2 ml h^{-1} and subsequently stained with APC-labelled anti-EpCAM, APC-labelled anti-cytokeratin, Alexa Fluor 488-labelled anti-CD45 antibody and DAPI. To measure the expression of c-Myc and vimentin mRNAs, the remaining supernatant solution was incubated with 20 µl of MNP-labelled EpCAM antibody for 30 min at room temperature. The cells were loaded into a cell-extraction microfluidic device[57] at a flow rate of 8 ml h^{-1}. After washing, the Tygon tubing connecting the zones was cut and the cells were gently pipetted out the device and stored at −80 °C before analysis by quantitative PCR with reverse transcription.

Analysis of intracellular proteins in clinical specimens. Patients with metastatic CRPC were recruited from the Princess Margaret Hospital according to the University of Toronto Research Ethics Board approval protocol. All patients were enrolled after giving informed consent. Ten millilitre samples of peripheral blood were collected from patients with CRPC in CellSearch tubes containing EDTA. All the samples were analysed within 24 h after collection. A set of patient blood samples ($n = 6$) and 1 healthy control were analysed to determine the applicability of the approach for the analysis of c-Myc and vimentin in CTCs. Mononuclear cells were isolated using the Ficoll method and subsequently suspended in 2 ml DPBS/DTT. For intracellular protein analysis, 200 µl of the supernatant was incubated with 200 µl of 8% PFA in DPBS/DTT for 15 min at 37 °C. After centrifugation, the cells were incubated with 100 µl of 0.3% Triton X-100 in DPBS/DTT for 10 min at room temperature. Afterwards, the cells were gently shaken with 5 µl of the DNA-conjugated antibody (specific for c-Myc or vimentin) for 30 min at room temperature. After centrifugation, the cells were gently shaken with a mixture of CP1 and CP2 in DPBS/DTT (100 µl each) for 3 h at room temperature. To determine the total number of cells in the sample, 200 µl of the supernatant were incubated with 20 µl MNP-labelled EpCAM antibody for 30 min at room temperature. The cells were loaded into the microfluidic device at a flow rate of 2 ml h^{-1} and subsequently stained with APC-labelled anti-EpCAM, APC-labelled anti-cytokeratin, Alexa Fluor 488-labelled anti-CD45 antibody and DAPI. To measure the expression of c-Myc and vimentin mRNAs, the remaining supernatant solution was incubated with 20 µl MNP-labelled EpCAM antibody for 30 min at room temperature. The cells were loaded into a cell-extraction microfluidic device[57] at a flow rate of 8 ml h^{-1}. After washing, the Tygon tubing connecting the zones was cut and the cells were gently pipetted out from the device and stored at −80 °C before analysis by quantitative PCR with reverse transcription.

Pancreatic cancer xenografts. All animal experiments were carried out in accordance with the protocol approved by the University of Toronto Animal Care Committee. Female athymic nude *Foxn1*^{nu} mice at 6–8 weeks of age were purchased from Envigo and maintained at the University of Toronto animal facility. Tumour xenografts were generated by injecting 5×10^6 Capan1 or Panc1 cells in 0.1 ml of PBS subcutaneously into the flanks of each mouse. Tumour volumes were measured twice per week using tumour volume = (length/2) × (width)^2. After one week, the tumour-bearing mice were randomly divided into control and treated groups ($n = 3$). Mice in the treated group received 50 mg kg^{-1} olaparib every other day for 4 weeks. Mice in the control group received only the vehicle. At day 7, 22 and 37, blood samples were collected from both treated and control mice by cardiac puncture under anaesthesia. All blood samples were collected in BD Vacutainer blood collection tubes containing EDTA (BD Biosciences). A total of 1 ml whole blood was collected from each mouse. The mononuclear cells were isolated using the Ficoll method and subsequently suspended in 600 µl DPBS/DTT. For intracellular protein analysis, 400 µl supernatant was incubated with 400 µl of 8% PFA in DPBS/DTT for 15 min at 37 °C. After centrifugation, the cells were incubated with 100 µl of 0.3% Triton X-100 in DPBS/DTT for 10 min at room temperature. After adding 100 µl DPBS/DTT, the cells were gently shaken with 5 µl DNA-conjugated antibody (specific for N terminus or C terminus of BRCA2 protein) for 30 min at room temperature. After centrifugation, the cells were gently shaken with a mixture of CP1 and CP2 in DPBS/DTT (100 µl each) for 3 h at room temperature. To determine the total number of cells in the sample, the remaining 200 µl of the supernatant was incubated with 20 µl MNP-labelled EpCAM antibody for 30 min at room temperature. The cells were loaded into the microfluidic device at a flow rate of 2 ml h^{-1} and subsequently stained with APC-labelled anti-EpCAM, APC-labelled anti-cytokeratin, Alexa Fluor 488-labelled anti-CD45 antibody and DAPI.

Statistical analyses. All statistical analyses were performed using the GraphPad Prism software. The specifics of the statistical tests and number of replicates are stated in the figure legends. The threshold for significance in all tests was $P < 0.05$.

Reporting summary. Further information on research design is available in the Nature Research Reporting Summary linked to this article.

Data availability

The main data supporting the results in this study are available within the paper and its Supplementary Information. The raw and analysed datasets generated during the study are too large to be publicly shared, but are available for research purposes from the corresponding authors on reasonable request.

Received: 31 October 2018; Accepted: 23 June 2020;
Published online: 27 July 2020

References

1. Alix-Panabieres, C. & Pantel, K. Challenges in circulating tumour cell research. *Nat. Rev. Cancer* **14**, 623–631 (2014).
2. Nagrath, S. et al. Isolation of rare circulating tumour cells in cancer patients by microchip technology. *Nature* **450**, 1235–1239 (2007).
3. Yoon, H. J. et al. Sensitive capture of circulating tumour cells by functionalized graphene oxide nanosheets. *Nat. Nanotechnol.* **8**, 735–741 (2013).
4. Zhao, W. et al. Bioinspired multivalent DNA network for capture and release of cells. *Proc. Natl Acad. Sci. USA* **109**, 19626–19631 (2012).
5. Stott, S. L. et al. Isolation of circulating tumor cells using a microvortex-generating herringbone-chip. *Proc. Natl Acad. Sci. USA* **107**, 18392–18397 (2010).
6. Ozkumur, E. et al. Inertial focusing for tumor antigen-dependent and -independent sorting of rare circulating tumor cells. *Sci. Transl. Med.* **5**, 179ra147 (2013).
7. Lee, A. et al. All-in-one centrifugal microfluidic device for size-selective circulating tumor cell isolation with high purity. *Anal. Chem.* **86**, 11349–11356 (2014).
8. Kim, T. H. et al. FAST: size-selective, clog-free isolation of rare cancer cells from whole blood at a liquid–liquid interface. *Anal. Chem.* **89**, 1155–1162 (2017).
9. Adams, A. A. et al. Highly efficient circulating tumor cell isolation from whole blood and label-free enumeration using polymer-based microfluidics with an integrated conductivity sensor. *J. Am. Chem. Soc.* **130**, 8633–8641 (2008).
10. Zhang, Y., Zhou, L. & Qin, L. High-throughput 3D cell invasion chip enables accurate cancer metastatic assays. *J. Am. Chem. Soc.* **136**, 15257–15262 (2014).
11. Zhang, Y., Zhang, W. & Qin, L. Mesenchymal-mode migration assay and antimetastatic drug screening with high-throughput microfluidic channel networks. *Angew. Chem. Int. Ed.* **53**, 2344–2348 (2014).
12. Toriello, N. M. et al. Integrated microfluidic bioprocessor for single-cell gene expression analysis. *Proc. Natl Acad. Sci. USA* **105**, 20173–20178 (2008).
13. Reyes, E. E. et al. Quantitative characterization of androgen receptor protein expression and cellular localization in circulating tumor cells from patients with metastatic castration-resistant prostate cancer. *J. Transl. Med.* **12**, 313 (2014).
14. Ciaccio, M. F., Wagner, J. P., Chuu, C. P., Lauffenburger, D. A. & Jones, R. B. Systems analysis of EGF receptor signaling dynamics with microwestern arrays. *Nat. Methods* **7**, 148–155 (2010).
15. Rimm, D. L. What brown cannot do for you. *Nat. Biotechnol.* **24**, 914–916 (2006).
16. Liu, Y. et al. Modulation of fluorescent protein chromophores to detect protein aggregation with turn-on fluorescence. *J. Am. Chem. Soc.* **140**, 7381–7384 (2018).
17. Pollock, S. B. et al. Highly multiplexed and quantitative cell-surface protein profiling using genetically barcoded antibodies. *Proc. Natl Acad. Sci. USA* **115**, 2836–2841 (2018).
18. Engelen, W., Meijer, L. H., Somers, B., de Greef, T. F. & Merkx, M. Antibody-controlled actuation of DNA-based molecular circuits. *Nat. Commun.* **8**, 14473 (2017).
19. Fan, R. et al. Integrated barcode chips for rapid, multiplexed analysis of proteins in microliter quantities of blood. *Nat. Biotechnol.* **26**, 1373–1378 (2008).
20. Nam, J. M., Thaxton, C. S. & Mirkin, C. A. Nanoparticle-based bio-bar codes for the ultrasensitive detection of proteins. *Science* **301**, 1884–1886 (2003).
21. Angelo, M. et al. Multiplexed ion beam imaging of human breast tumors. *Nat. Med.* **20**, 436–442 (2014).
22. Rissin, D. M. et al. Single-molecule enzyme-linked immunosorbent assay detects serum proteins at subfemtomolar concentrations. *Nat. Biotechnol.* **28**, 595–599 (2010).
23. de la Rica, R. & Stevens, M. M. Plasmonic ELISA for the ultrasensitive detection of disease biomarkers with the naked eye. *Nat. Nanotechnol.* **7**, 821–824 (2012).
24. Xue, M. et al. Chemical methods for the simultaneous quantitation of metabolites and proteins from single cells. *J. Am. Chem. Soc.* **137**, 4066–4069 (2015).
25. Gerdtsson, T. et al. Multiplex protein detection on circulating tumor cells from liquid biopsies using imaging mass cytometry. *Converg. Sci. Phys. Oncol.* **4**, 015002 (2018).
26. Hughes, A. J. et al. Single-cell western blotting. *Nat. Methods* **11**, 749–755 (2014).
27. Sinkala, E. et al. Profiling protein expression in circulating tumour cells using microfluidic western blotting. *Nat. Commun.* **8**, 14622 (2017).
28. Poudineh, M. et al. Tracking the dynamics of circulating tumour cell phenotypes using nanoparticle-mediated magnetic ranking. *Nat. Nanotechnol.* **12**, 274–281 (2017).
29. Labib, M. et al. Single-cell mRNA cytometry via sequence-specific nanoparticle clustering and trapping. *Nat. Chem.* **10**, 489–495 (2018).
30. Herold, S., Herkert, B. & Eilers, M. Facilitating replication under stress: an oncogenic function of MYC? *Nat. Rev. Cancer* **9**, 441–444 (2009).
31. Dang, C. V. MYC on the path to cancer. *Cell* **149**, 22–35 (2012).
32. Beaulieu, M. E. et al. Intrinsic cell-penetrating activity propels Omomyc from proof of concept to viable anti-MYC therapy. *Sci. Transl. Med.* **11**, eaar5012 (2019).
33. Burke, A. J., Ali, H., O'Connell, E., Sullivan, F. J. & Glynn, S. A. Sensitivity profiles of human prostate cancer cell lines to an 80 kinase inhibitor panel. *Anticancer Res.* **36**, 633–641 (2016).
34. Lakshman, M. et al. Dietary genistein inhibits metastasis of human prostate cancer in mice. *Cancer Res.* **68**, 2024–2032 (2008).
35. Thiery, J. P. Epithelial–mesenchymal transitions in tumour progression. *Nat. Rev. Cancer* **2**, 442–454 (2002).
36. Lindsay, C. R. et al. Vimentin and Ki67 expression in circulating tumour cells derived from castrate-resistant prostate cancer. *BMC Cancer* **16**, 168 (2016).
37. Ray Chaudhuri, A. & Nussenzweig, A. The multifaceted roles of PARP1 in DNA repair and chromatin remodelling. *Nat. Rev. Mol. Cell Biol.* **18**, 610–621 (2017).
38. Schiewer, M. J. et al. Dual roles of PARP-1 promote cancer growth and progression. *Cancer Discov.* **2**, 1134–1149 (2012).
39. Kosaka, T. et al. The prognostic significance of OCT4 expression in patients with prostate cancer. *Hum. Pathol.* **51**, 1–8 (2016).
40. Salem, A. F., Whitaker-Menezes, D., Howell, A., Sotgia, F. & Lisanti, M. P. Mitochondrial biogenesis in epithelial cancer cells promotes breast cancer tumor growth and confers autophagy resistance. *Cell Cycle* **11**, 4174–4180 (2012).
41. Gao, L. et al. Androgen receptor promotes ligand-independent prostate cancer progression through c-Myc upregulation. *PLoS ONE* **8**, e63563 (2013).
42. Wu, M. et al. Proteome analysis of human androgen-independent prostate cancer cell lines: variable metastatic potentials correlated with vimentin expression. *Proteomics* **7**, 1973–1983 (2007).
43. Stratton, M. R., Campbell, P. J. & Futreal, P. A. The cancer genome. *Nature* **458**, 719–724 (2009).
44. Tran, C. et al. Development of a second-generation antiandrogen for treatment of advanced prostate cancer. *Science* **324**, 787–790 (2009).
45. Scher, H. I. et al. Antitumour activity of MDV3100 in castration-resistant prostate cancer: a phase 1–2 study. *Lancet* **375**, 1437–1446 (2010).
46. Watson, P. A., Arora, V. K. & Sawyers, C. L. Emerging mechanisms of resistance to androgen receptor inhibitors in prostate cancer. *Nat. Rev. Cancer* **15**, 701–711 (2015).
47. Sinkevicius, K. W. et al. Neurotrophin receptor TrkB promotes lung adenocarcinoma metastasis. *Proc. Natl Acad. Sci. USA* **111**, 10299–10304 (2014).
48. Chen, Y. & Chi, P. Basket trial of TRK inhibitors demonstrates efficacy in TRK fusion-positive cancers. *J. Hematol. Oncol.* **11**, 78–78 (2018).
49. Wylie, A. A. et al. The allosteric inhibitor ABL001 enables dual targeting of BCR–ABL1. *Nature* **543**, 733–737 (2017).
50. Holderfield, M., Deuker, M. M., McCormick, F. & McMahon, M. Targeting RAF kinases for cancer therapy: BRAF-mutated melanoma and beyond. *Nat. Rev. Cancer* **14**, 455–467 (2014).
51. Hauschild, A. et al. Dabrafenib in BRAF-mutated metastatic melanoma: a multicentre, open-label, phase 3 randomised controlled trial. *Lancet* **380**, 358–365 (2012).
52. Rebbeck, T. R. et al. Prophylactic oophorectomy in carriers of BRCA1 or BRCA2 mutations. *N. Engl. J. Med.* **346**, 1616–1622 (2002).
53. Jeyasekharan, A. D. et al. A cancer-associated BRCA2 mutation reveals masked nuclear export signals controlling localization. *Nat. Struct. Mol. Biol.* **20**, 1191–1198 (2013).
54. Eriksson, I., Wettermark, B. & Bergfeldt, K. Real-world use and outcomes of olaparib: a population-based cohort study. *Target. Oncol.* **13**, 725–733 (2018).
55. Mateo, J. et al. DNA-repair defects and olaparib in metastatic prostate cancer. *N. Engl. J. Med.* **373**, 1697–1708 (2015).
56. Rowe, B. P. & Glazer, P. M. Emergence of rationally designed therapeutic strategies for breast cancer targeting DNA repair mechanisms. *Breast Cancer Res.* **12**, 203 (2010).
57. Green, B. J. et al. Isolation of phenotypically distinct cancer cells using nanoparticle-mediated sorting. *ACS Appl. Mater. Interfaces* **9**, 20435–20443 (2017).

Acknowledgements

This work was supported by the Canadian Institutes of Health Research (grant no. FDN-148415), the Natural Sciences and Engineering Research Council of Canada (grant no. 2016-06090), the Province of Ontario though the Ministry of Research, Innovation and Science (grant no. RE05-009) and the National Cancer Institute of the National Institutes of Health (grant no. 1R33CA204574). The content is solely the responsibility of the authors and does not necessarily represent the official views of the National Institutes of Health or the other funding agencies. We thank A. Joshua for providing the clinical specimens.

Author contributions

M.L., S.O.K. and E.H.S. conceived and designed the experiments. M.L., Z.W., S.U.A., R.M.M., B.D. and B.G. performed the experiments and analysed the data. All authors discussed the results and contributed to the preparation and editing of the manuscript.

Competing interests

The authors declare no competing interests.

Additional information

Supplementary information is available for this paper at https://doi.org/10.1038/s41551-020-0590-1.

Correspondence and requests for materials should be addressed to S.O.K.

Reprints and permissions information is available at www.nature.com/reprints.

Publisher's note Springer Nature remains neutral with regard to jurisdictional claims in published maps and institutional affiliations.

nature research

Corresponding author(s): Shana O. Kelley

Last updated by author(s): Jun 17, 2020

Reporting Summary

Nature Research wishes to improve the reproducibility of the work that we publish. This form provides structure for consistency and transparency in reporting. For further information on Nature Research policies, see our Editorial Policies and the Editorial Policy Checklist.

Statistics

For all statistical analyses, confirm that the following items are present in the figure legend, table legend, main text, or Methods section.

n/a	Confirmed	
☐	☒	The exact sample size (*n*) for each experimental group/condition, given as a discrete number and unit of measurement
☐	☒	A statement on whether measurements were taken from distinct samples or whether the same sample was measured repeatedly
☐	☒	The statistical test(s) used AND whether they are one- or two-sided *Only common tests should be described solely by name; describe more complex techniques in the Methods section.*
☒	☐	A description of all covariates tested
☒	☐	A description of any assumptions or corrections, such as tests of normality and adjustment for multiple comparisons
☐	☒	A full description of the statistical parameters including central tendency (e.g. means) or other basic estimates (e.g. regression coefficient) AND variation (e.g. standard deviation) or associated estimates of uncertainty (e.g. confidence intervals)
☒	☐	For null hypothesis testing, the test statistic (e.g. *F*, *t*, *r*) with confidence intervals, effect sizes, degrees of freedom and *P* value noted *Give P values as exact values whenever suitable.*
☒	☐	For Bayesian analysis, information on the choice of priors and Markov chain Monte Carlo settings
☒	☐	For hierarchical and complex designs, identification of the appropriate level for tests and full reporting of outcomes
☒	☐	Estimates of effect sizes (e.g. Cohen's *d*, Pearson's *r*), indicating how they were calculated

Our web collection on statistics for biologists contains articles on many of the points above.

Software and code

Policy information about availability of computer code

Data collection	Chip design: AutoCAD 2015 Sorting: Nikon Elements Flow cytometry: FACSDIVA
Data analysis	Microsoft Excel 2016 (16.0.1230.20232), GraphPad prism v8.0.2 (263), and FlowJo_V10.

For manuscripts utilizing custom algorithms or software that are central to the research but not yet described in published literature, software must be made available to editors and reviewers. We strongly encourage code deposition in a community repository (e.g. GitHub). See the Nature Research guidelines for submitting code & software for further information.

Data

Policy information about availability of data

All manuscripts must include a data availability statement. This statement should provide the following information, where applicable:

- Accession codes, unique identifiers, or web links for publicly available datasets
- A list of figures that have associated raw data
- A description of any restrictions on data availability

The main data supporting the results in this study are available within the paper and its Supplementary Information. The raw and analysed datasets generated during the study are too large to be publicly shared, yet they are available for research purposes from the corresponding authors on reasonable request.

Field-specific reporting

Please select the one below that is the best fit for your research. If you are not sure, read the appropriate sections before making your selection.

☒ Life sciences ☐ Behavioural & social sciences ☐ Ecological, evolutionary & environmental sciences

For a reference copy of the document with all sections, see nature.com/documents/nr-reporting-summary-flat.pdf

Life sciences study design

All studies must disclose on these points even when the disclosure is negative.

Sample size	No sample-size calculations were performed, and sample sizes were arbitrarily chosen according to conventions in the field. The number of replicates was at least three biological replicates (that is, independent experiments) and/or at least three technical replicates (that is, repeated measurements of the same original sample). Due to limited sample availability, a single measurement was carried out for c-Myc and vimentin protein in clinical samples as well as prostate cancer xenografts.
Data exclusions	No data were excluded from any experiments and from any of the figures.
Replication	All attempts for replication were reproducible. All replicates are shown in the main figures and the supplementary figures.
Randomization	Randomization was performed in the human and animal studies.
Blinding	All patients were enrolled subsequent to informed consent, with no self-selection bias.

Reporting for specific materials, systems and methods

We require information from authors about some types of materials, experimental systems and methods used in many studies. Here, indicate whether each material, system or method listed is relevant to your study. If you are not sure if a list item applies to your research, read the appropriate section before selecting a response.

Materials & experimental systems

n/a	Involved in the study
☐	☒ Antibodies
☐	☒ Eukaryotic cell lines
☒	☐ Palaeontology and archaeology
☐	☒ Animals and other organisms
☐	☒ Human research participants
☒	☐ Clinical data
☒	☐ Dual use research of concern

Methods

n/a	Involved in the study
☒	☐ ChIP-seq
☐	☒ Flow cytometry
☒	☐ MRI-based neuroimaging

Antibodies

Antibodies used

Dilutions and conditions of use are provided in the Methods section.
- EpCAM antibody conjugated with magnetic nanoparticles (monoclonal, Miltenyi Biotec, Cat.# 130-061-101, RRID:AB_2832928, multiple lots)
- APC-labelled cytokeratin antibody (clone C-11, GeneTex, Cat.# GTX80205, RRID:AB_11171332, multiple lots)
- APC-labelled EpCAM antibody (clone REA764, Miltenyi Biotec, Cat.# 130-111-000, RRID:AB_2657497, multiple lots)
- AF488-labelled EpCAM antibody (clone HI30, Invitrogen, Cat.# MHCD4520, RRID:AB_1475770, multiple lots)
- Rabbit IgG isotype control antibody (Invitrogen, Cat.# 02-6102, RRID:AB_253293, multiple lots)
- Mouse IgG isotype control antibody (Invitrogen, Cat.# 10400C, RRID:AB_2532980, multiple lots)
- FITC-labelled mouse anti-rabbit antibody (polyclonal, Invitrogen, Cat.# 31584, RRID: AB_228242, multiple lots)
- APC-labelled Goat anti-Rabbit antibody (polyclonal, R&D Biosystems, Cat.# F0111, RRID:AB_573127, multiple lots)
- APC-labelled Goat anti-Mouse antibody (polyclonal, R&D Biosystems, Cat.# F0101B, RRID:AB_622013, multiple lots)
- Biotin-labelled c-Myc antibody (polyclonal, Bioss Inc., Cat.# bs-0842R-Biotin, RRID:AB_11096765, multiple lots)
- Vimentin antibody (polyclonal, Bioss Inc., Cat.# bs-0756R, RRID:AB_10855343, multiple lots)
- Oct4 antibody (polyclonal, Bioss Inc., Cat.# bs-1111R, RRID:AB_10855418, multiple lots)
- ARV7 antibody (clone RM7, RevMAb Biosceinces, Cat.# 31-1109-00, RRID:AB_2716436, multiple lots)
- BCR-ABL1 antibody (clone 7C6, Abcam, Cat.# ab187831, RRID:AB_2536861, multiple lots)
- PARP1 antibody (polyclonal, LifeSpan Biosciences Inc., Cat.# LS-C745005, RRID:AB_2160747, multiple lots)
- BRAFv600E antibody (clone 7C6, RevMAb Biosceinces, Cat.# 31-1042-00, RRID:AB_2716429, multiple lots)
- TrkA antibody (clone EP1058Y, Abcam, Cat.# ab76291, RRID:AB_1524514, multiple lots)
- TrkB antibody (clone EPR1294, Abcam, Cat.# ab134155, multiple lots)
- BRCA2 (N-terminus) antibody (polyclonal, Abcam, Cat.# ab75335, RRID:AB_2067758, multiple lots)
- BRCA2 (C-terminus) antibody (polyclonal, Arigo Biolaboratories Corp., Cat.# ARG10523, multiple lots)

- Pan cytokeratin antibody (polyclonal, Bioss Inc., Cat.# bs-1712R, RRID:AB_10855057, multiple lots)
- c-Myc antibody (polyclonal, Bioss Inc., Cat.# bs-4963R, multiple lots)
- KRAS 2B antibody (polyclonal, Proteintech, Cat.# 16155-1-AP, RRID:AB_2134119, multiple lots)
- POLRMT antibody (polyclonal, USBiological, Cat.# 489004 Pab, multiple lots)

Validation

All antibodies used in this study were validated by the manufacturers, and validation data are available online at the manufacturers' websites. The antibodies were validated by flow cytometry and/or Western blotting and/or immunocytochemistry and/or immunohistochemistry. Details about the used antibodies and the suppliers are provided in the previous section.

Eukaryotic cell lines

Policy information about cell lines

Cell line source(s)	22Rv1, PC3, PC3M, DU145, LNCaP, 562, Jurkat, MDA-MB-231, HT29, H460, Panc1, and Capan1 were purchased from ATCC.
Authentication	All cell lines were authenticated by STR profiling at the Centre for Applied Genomics (TCAG) at the Hospital for Sick Children (SickKids) in Toronto.
Mycoplasma contamination	All cell lines were routinely tested and confirmed negative for mycoplasma contamination.
Commonly misidentified lines (See ICLAC register)	None of the cell lines used in this study are listed as commonly misidentified.

Animals and other organisms

Policy information about studies involving animals; ARRIVE guidelines recommended for reporting animal research

Laboratory animals	Male athymic nude mice (6-8 weeks old) and female Athymic Nude-Foxn1nu mice at 6-8 weeks of age were purchased from Envigo and maintained at the University of Toronto animal facility.
Wild animals	The study did not involve wild animals.
Field-collected samples	The study did not involve samples collected from the field.
Ethics oversight	All animal experiments were carried out in accordance with the protocol approved by the University of Toronto Animal Care Committee.

Note that full information on the approval of the study protocol must also be provided in the manuscript.

Human research participants

Policy information about studies involving human research participants

Population characteristics	Metastatic castration-resistant prostate cancer (CRPC) patients were recruited from the Princess Margaret Hospital according to the University of Toronto Research Ethics Board approval protocol.
Recruitment	All patients were enrolled subsequent to informed consent with no self-selection bias.
Ethics oversight	The study protocol was approved by the University of Toronto Research Ethics Board.

Note that full information on the approval of the study protocol must also be provided in the manuscript.

Flow Cytometry

Plots

Confirm that:

☒ The axis labels state the marker and fluorochrome used (e.g. CD4-FITC).

☒ The axis scales are clearly visible. Include numbers along axes only for bottom left plot of group (a 'group' is an analysis of identical markers).

☒ All plots are contour plots with outliers or pseudocolor plots.

☒ A numerical value for number of cells or percentage (with statistics) is provided.

Methodology

Sample preparation	Cell lines were dissociated with 0.125% trypsin. The cells were incubated with the blocking buffer (2% BSA in PBS) for 30 min on ice. The cells were fixed with 4% PFA for 10 min on ice. For cell-surface protein analysis, the cells were incubated with the primary antibody for 30 min at room temperature. The cells were then incubated with the fluorescently-labelled antibody for 30 min in the dark. For intracellular protein analysis, the cells were permeabilized with 0.2% TX-100 for 10 min at room temperature after the fixation step and before incubation with the antibodies. Prior to analysis, the cells were washed three

	times with 2% BSA in PBS.
Instrument	FACSCanto flow cytometer (BD Biosciences, US).
Software	Data were acquired by using FACSDIVA software v8.0-8.1 (BD Biosciences)and analyzed by using FlowJo_V10 software.
Cell population abundance	Provided in Methods.
Gating strategy	Single-parameter histogram was used. All measurements were carried out relative to unstained control. In addition, all measurements were repeated using isotype controls.

☒ Tick this box to confirm that a figure exemplifying the gating strategy is provided in the Supplementary Information.